HHS Public Access

Author manuscript

ACS Chem Biol. Author manuscript; available in PMC 2023 December 16.

Published in final edited form as:

ACS Chem Biol. 2022 December 16; 17(12): 3450–3457. doi:10.1021/acschembio.2c00591.

Amyotrophic Lateral Sclerosis-Associated Mutants of SOD1 Modulate miRNA Biogenesis through Aberrant Interactions with Exportin 5

Xingyuan Chen,
Environmental Toxicology Graduate Program, University of California, Riverside, California 92502, United States

Xiaomei He,
Department of Chemistry, University of California, Riverside, California 92502, United States

Yen-Yu Yang,
Department of Chemistry, University of California, Riverside, California 92502, United States

Yinsheng Wang
Environmental Toxicology Graduate Program and Department of Chemistry, University of California, Riverside, California 92502, United States

Abstract

Mutations in the *SOD*1 (superoxide dismutase 1) gene are associated with amyotrophic lateral sclerosis (ALS), a fatal neurodegenerative disease. By employing ascorbate peroxidase-based proximity labeling, coupled with LC–MS/MS analysis, we uncovered 43 and 24 proteins exhibiting higher abundance in the proximity proteomes of $SOD1^{G85R}$ and $SOD1^{G93A}$, respectively, than that of wild-type SOD1. Immunoprecipitation followed by western blot analysis indicated the preferential binding of one of these proteins, exportin 5 (XPO5), toward the two mutants of SOD1 over the wild-type counterpart. In line with the established function of XPO5 in pre-miRNA transport, we observed diminished nucleocytoplasmic transport of pre-miRNAs in cells with ectopic expression of the two SOD1 mutants over those expressing the wild-type protein. On the other hand, RT-qPCR results revealed significant elevations in mature miRNA in cells expressing the two SOD1 mutants, which are attributed to the diminished inhibitory effect of XPO5 on Dicer-mediated cleavage of pre-miRNA to mature miRNA. Together, our chemoproteomic approach led to the revelation of a novel mechanism through which ALS-associated mutants of SOD1 perturb miRNA biogenesis, that is, through aberrant binding toward XPO5.

Corresponding Author: Yinsheng Wang – Environmental Toxicology Graduate Program and Department of Chemistry, University of California, Riverside, California 92502, United States; Phone: (951) 827-2700; yinsheng@ucr.edu; Fax: (951) 827-4713.

Supporting Information

The Supporting Information is available free of charge at https://pubs.acs.org/doi/10.1021/acschembio.2c00591.
List of primers used, LC–MS/MS quantification results, and gene ontology analysis results (PDF)

Complete contact information is available at: https://pubs.acs.org/10.1021/acschembio.2c00591

The authors declare no competing financial interest.

Graphical Abstract

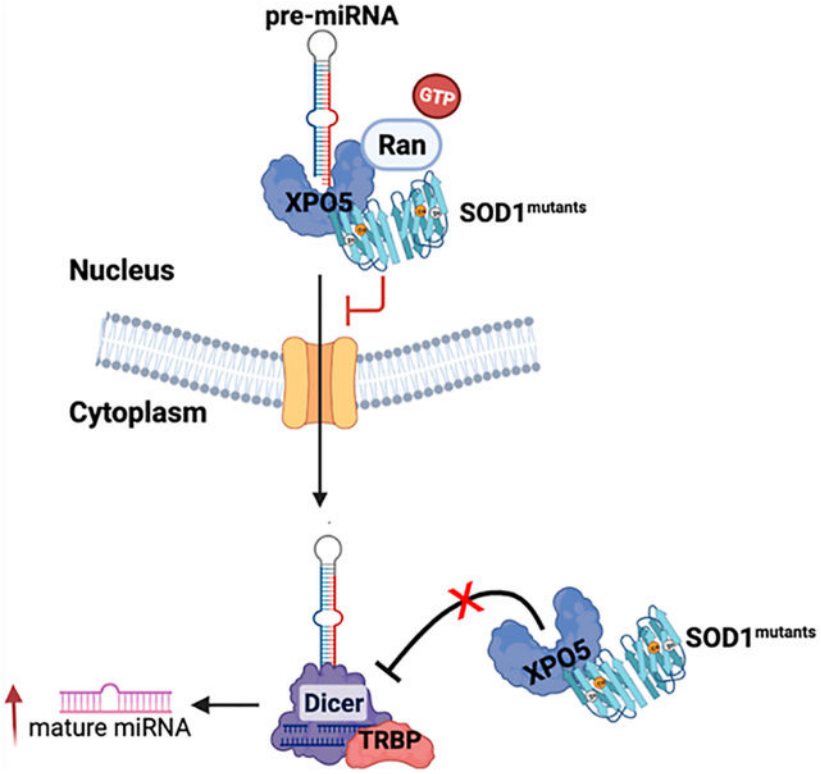

INTRODUCTION

Amyotrophic lateral sclerosis (ALS) is a progressive, fatal neurodegenerative disorder manifested by the degeneration of motor neurons in the brain and spinal cord, resulting in paralysis and death.[1] The onset of ALS usually occurs in the late middle life at around 55 years old, starting with insidious muscle weakness and spreading to progressive muscle atrophy, with survival being limited to 2–3 years after disease onset.[2] Mechanisms such as mitochondria dysfunction, altered axonal transport, disturbances in RNA metabolism, inflammation, proteasome impairment, and oxidative stress have been implicated in ALS pathologies.[1,3] More than 20 ALS-linked genes have been identified to date, including pathogenic variants of *SOD*1, *FUS*, *C*9*ORF*72, and *TARDBP*, which are among the most extensively studied.[4]

Approximately 10% of ALS patients are inherited (familial), among which about 20% arise from mutations in the SOD1 gene encoding the Cu/Zn-superoxide dismutase, a free radical-scavenging enzyme protecting cells against oxidative stress.[5] More than 200 ALS-associated mutations have been found for SOD1, with Gly-to-Ala mutation at position 93 (G93A) and Gly-to-Arg mutation at position 85 (G85R) being the most extensively investigated.[6,7] Previous studies documented protein aggregation as one of the most prominent features of ALS-associated SOD1 mutations, suggesting a loss of effective folding and degradation of the mutant SOD1 proteins.[8] Nevertheless, little is known about how those mutations of SOD1 found in ALS patients modulate its interactions with other cellular proteins.

In recent years, proximity-based labeling methods, including biotin ligase $BirA^{R118G}$ (BioID), engineered ascorbate peroxidase (APEX), and TurboID, have been widely employed to examine protein–protein interactions in the native cellular environment.[9–11] Both BioID and APEX rely on the generation of a reactive biotin derivative to label proximal endogenous proteins.[9,10] However, compared with BioID, APEX exhibits much faster reaction kinetics and shorter labeling time, which enable the study of short-lived cell states.[12]

In this study, we employed APEX-based proximity labeling using the improved second-generation enzyme APEX2[10] in conjunction with liquid chromatography–tandem mass spectrometry (LC–MS/MS) analysis, to examine how two ALS-associated mutations of SOD1, that is, the G93A and G85R substitutions,[12] perturb the interactions of SOD1 with other cellular proteins. We uncovered that the two ALS-associated mutants elicited alterations in a number of proteins in the proximity proteome of SOD1, including a markedly elevated presence of exportin 5 (XPO5). We also demonstrated that the aberrant interactions of SOD1 mutants with XPO5 resulted in the compromised export of pre-miRNA and elevated biogenesis of mature miRNA.

EXPERIMENTAL SECTION

Cell Culture.

HEK293T cells (ATCC) and N2a cells (Thermo Fisher) were maintained in Dulbecco's modified Eagle medium supplemented with 10% fetal bovine serum (Invitrogen) and 1% penicillin/streptomycin (at 10,000 U/mL, Thermo Fisher). The cells were cultured at an 80% confluency under 37 °C in a humidified atmosphere containing 5% CO_2.

Plasmids.

Plasmids for wild-type (WT) SOD1 (plasmid #26397), $SOD1^{G85R}$ (plasmid #26400), and $SOD1^{G93A}$ (plasmid#26401) were obtained from Addgene. The plasmids for APEX experiments were engineered from Mito-V5-APEX2 (Addgene, plasmid #72480) by removing the region encoding the mitochondria matrix targeting sequence and by inserting NotI, EagI, EaeI, BsiEI, ApoI, EcoRI, NheI, and BmtI restriction recognition sites to generate the V5-APEX2 vector (Figure S1). The coding sequences of WT and mutant SOD1 were subsequently cloned into the NotI and NheI restriction sites of the V5-APEX2 vector on the N-terminus of the V5 tag to generate the $SOD1^{WT}$-APEX2, $SOD1^{G85R}$-APEX2, and $SOD1^{G93A}$-APEX2 plasmids. The $SOD1^{WT}$-Flag, $SOD1^{G85R}$-Flag, and $SOD1^{G93A}$-Flag for expressing SOD1 variants with three tandem repeats of the Flag tag being fused on the C-terminus were constructed by inserting the coding sequences of the SOD1 variants into the HindIII and Xbal restriction sites of the pRK7 3× Flag vector (Addgene, plasmid #8996). All constructs were confirmed by Sanger sequencing.

Cell Lysis and Proteomic Sample Preparation.

APEX labeling was performed at 24 h after the transfection of HEK293T cells with the aforementioned SOD1-APEX2 plasmids, following recently described procedures.[13] In brief, approximately 2×10^7 cells transfected with the plasmids were incubated with 500 μM

biotin phenol in a complete medium for 30 min in a 37 °C incubator, followed by incubation with 1.0 mM H_2O_2 for 1 min to induce biotinylation. To quench the reaction, the cells were washed with a solution containing 5 mM 6-hydroxy-2,5,7,8-tetramethylchroman-2-carboxylic acid (Trolox), 10 mM sodium ascorbate, and 10 mM sodium azide in phosphate-buffered saline (PBS), followed by washing with PBS twice. The cells were lysed in 500 μL of 7.0 M urea containing 1% protease inhibitor cocktail (Sigma) in 50 mM Tris buffer (pH 7.5) and the above-described quenching buffer. The mixtures were briefly vortexed and rotated for 20 min to completely lyse the cells, followed by centrifugation at 13,000 rpm at room temperature for 30 min to remove the cell debris.

For streptavidin pull-down, 1 mg of the protein lysate was incubated with streptavidin-conjugated agarose beads (Thermo Fisher) at room temperature for 2 h. The beads were subsequently washed five times with 500 μL of 7.0 M urea. To elute the biotinylated proteins, the beads were incubated with a 3× sodium dodecyl sulfate (SDS)–polyacrylamide gel electrophoresis (PAGE) loading buffer containing 2 mM biotin at 95 °C for 5 min. The resulting proteins were resolved on a 10% SDS–PAGE gel, followed by the excision of gel bands in the molecular weight range of ≥15 kDa into 1 mm^3 cubes. The gel cubes were destained and dehydrated, followed by cysteine reduction and alkylation, where the gel pieces were incubated in 10 mM dithiothreitol and 55 mM iodoacetamide at 37 °C for 1 h and at room temperature in the dark for 20 min, respectively. The proteins were digested in gel with trypsin, and the resultant peptide mixture was dried in a Speed-vac and desalted using OMIX C18 pipette tips (Agilent Technologies).

The desalted peptides were dissolved in 0.1% formic acid and subjected to LC–MS/MS analysis on a Q Exactive Plus hybrid quadrupole-Orbitrap mass spectrometer (Thermo Fisher Scientific) coupled with an Ultimate 3000 UPLC system. Approximately 20% of the samples were loaded onto a 3 cm trapping column (150 μm i.d.) packed with ReproSil-Pur 120 C18-AQ resin (5 μm in particle size and 120 Å in pore size, Dr. Maisch GmbH HPLC), and the flow rate was 3 μL/min. The peptides were separated on a 20 cm fused silica analytical column (75 μm i.d.) packed with ReproSil-Pur 120 C18-AQ resin (3 μm in particle size and 120 Å in pore size). A 140 min linear gradient of 4.0–29.6% acetonitrile in 0.1% formic acid was employed for the separation, and the flow rate was 300 nL/min. The spray voltage was set at 2.0 kV. The mass spectrometer was operated in a data-dependent acquisition mode, where the 25 most abundant ions detected in MS were isolated and activated in the HCD cell at a collision energy of 28 to yield the MS/MS. The MS/MS spectra were acquired using an Orbitrap analyzer at a resolution of 17,500 and with an automatic gain control target of 1×10^5.

The raw LC–MS/MS data were processed using MaxQuant (version 2.0.1.0). The mass tolerance was set at 20 ppm for both MS and MS/MS. Cysteine carbamidomethylation was set as a fixed modification, and methionine oxidation and N-terminal acetylation were set as variable modifications. Peptides were filtered at a 1% false discovery rate (FDR), and a maximum of two trypsin missed cleavages were allowed. The match time window was 0.7 min between replicates. The mass spectra of peptides were searched using a target-decoy human UniProt database (UP000005640) for protein identification. The results were filtered

at 1% protein FDR. Normalized label-free quantification was used for protein quantification with a minimum ratio count of two.

The MS proteomics data have been deposited to the ProteomeXchange Consortium via the PRIDE[14] partner repository with the dataset identifier PXD035452 (username: reviewer_pxd035452@ebi.ac.uk; password: oleWYQkO).

Immunoprecipitation and Western Blot.

Approximately 2×10^7 cells were harvested and lysed in CelLytic M Cell Lysis reagent supplemented with a complete protease inhibitor cocktail (Sigma-Aldrich). The lysates were subjected to rotation at 4 °C for 15 min, followed by sonication using a Qsonica sonicator q125 (1/8 probe) for 15 s three times (42% amplitude, 15 s on/15 s off). After sonication, the cell lysates were rotated for another 15 min and then centrifuged at 13,000 rpm for 10 min at 4 °C. The supernatant was incubated with prewashed anti-Flag M2 beads at 4 °C for 2 h. The beads were washed three times with PBS-T (PBS buffer containing 0.05% Tween 20), and subsequently boiled in 2× SDS–PAGE loading buffer to elute the captured proteins for western blot analysis.

Antibodies recognizing human XPO5 (Proteintech, #28628–1-AP; 1:2000), SOD1 (Proteintech, #10269–1-AP; 1:4000), V5 (Proteintech, #14440–1-AP; 1:2000), streptavidin (Thermo Scientific, #S911), and lamin B1 (Proteintech, #12987–1-AP; 1:10000) were used as primary antibodies for western blot analysis. Goat antirabbit IgG (whole molecule)-peroxidase antibody (Sigma, #A0545; 1:4000) and *m*-IgGκ BP-HRP (Santa Cruz Biotechnology, #sc-516102; 1:4000) were employed as secondary antibodies. Anti-GAPDH (Santa Cruz Biotechnology, #sc-32233; 1:10000) was used for internal control (GAPDH) to confirm an equal amount of protein loading.

Real-Time-Quantitative PCR Analysis of Expression Levels for Pre-miRNA and Mature miRNA.

Pre-miRNAs were extracted by following previously published procedures.[15] Cells were seeded in six-well plates at a 35% confluence level and transfected with plasmids encoding $SOD1^{WT}$-Flag, $SOD1^{G85R}$-Flag, and $SOD1^{G93A}$-Flag the following day.

Cytosolic RNAs were extracted 24 h after transfection using cytoplasmic extraction reagents I and II, followed by the extraction of nuclear RNA from the cell pellet using 50 μL of nuclear extraction reagent (Thermo Scientific, #78833). Both cytosolic and nuclear RNAs were treated with 1 mL of TRIzol, followed by cDNA synthesis using a previously published method.[8] Approximately 2 μg RNA was denatured and annealed by incubating with random hexamer-containing reverse primers of the four mature miRNAs at 70 °C for 5 min. The resulting RNA was quickly placed on ice, followed by reverse transcription at 42 °C for 1 h and 75 °C for 15 min using 100 units of M-MLV reverse transcriptase (Promega), M-MLV buffer, dNTP mixture, and RNase inhibitor. Pre-miRNA primers and Luna Universal qPCR Master Mix were subsequently added to the mixture, followed by real-time quantitative PCR (RT-qPCR) analysis on a Bio-Rad iCycler system, with the running protocol being set at 95 °C for 3 min and 55 cycles at 95 °C for 15 s, 55 °C for

30 s, and 72 °C for 45 s. The primers are listed in Table S1. The levels of pre-miRNA were normalized to that of *GAPDH* mRNA.

Mature miRNA was isolated as described previously.[16] Cells were seeded in a six-well plate at a 35% confluence level and transfected with $SOD1^{WT}$-Flag, $SOD1^{G85R}$-Flag, and $SOD1^{G93A}$-Flag the following day. Total RNA was extracted at 24 h after transfection using TRIzol, followed by cDNA synthesis. In general, approximately 1 μg of RNA was reverse-transcribed by employing 100 units of M-MLV reverse transcriptase (Promega), 1 unit of poly(A) polymerase (New England Biolabs), and a 5′-tagged oligo$(dT)_{15}$ primer. After a 1 h incubation at 42 °C, the reverse transcriptase was deactivated by heating the mixture at 95 °C for 5 min. RT-qPCR experiments were performed using the Luna Universal qPCR Master Mix on a Bio-Rad iCycler system. The primers are listed in Table S1. The levels of mature miRNAs were normalized to the mRNA level of *GAPDH*.

RESULTS

APEX2 Labeling in Combination with LC–MS/MS for Assessing the Interactomes of $SOD1^{WT}$, $SOD1^{G85R}$, and $SOD1^{G93A}$.

In this study, we employed APEX labeling, coupled with LC–MS/MS, to explore the differences in interaction proteomes of $SOD1^{WT}$, $SOD1^{G85R}$, and $SOD1^{G93A}$ (Figure 1a). We first optimized the amounts of plasmids employed for the transfection so as to achieve a similar level of expression for $SOD1^{WT}$, $SOD1^{G85R}$, and $SOD1^{G93A}$, as suggested by western blot analysis (Figure 1b). We next performed APEX labeling, and our results from western blot analysis indicated that the biotin labeling efficiencies for $SOD1^{WT}$, $SOD1^{G85R}$, and $SOD1^{G93A}$ were similar (Figure 1c). In this vein, it is of note that western blot analysis only provided a semiquantitative assessment of protein expression.

The combination of APEX labeling with LC–MS/MS analysis revealed substantial (by at least 1.5-fold) enrichments of 43 and 24 proteins in the proximity proteomes of $SOD1^{G85R}$ and $SOD1^{G93A}$, respectively, relative to $SOD1^{WT}$ (Figure 1d,e). In addition, gene ontology analysis of the biological processes for the enriched proximity proteins of the two mutants showed perturbations in several important pathways, including tRNA aminoacylation for protein translation, regulation of macro-autophagy, phosphorylation, vesicle-mediated transport, ER to Golgi vesicle-mediated transport, and RNA splicing (Figure S2). In this vein, NOP56 was found to be enriched in the proximity proteome of $SOD1^{G85R}$ only and was a previously reported ALS-associated gene that is involved in ribosomal subunit assembly and pre-rRNA processing (Figure 1e).[17,18] Moreover, several proteins involved in RNA metabolism, such as XPO5, NONO, SRSF6, and YTHDC1, were detected only in the proximity proteomes of $SOD1^{G85R}$ and $SOD1^{G93A}$ but not that of $SOD1^{WT}$. SEC23A and SEC23B, which are intracellular trafficking proteins and previously shown to interact with $SOD1^{G85R}$,[19] were also detected in our APEX labeling experiments (Tables S2 and S3).

Our results also showed that 221 and 426 proteins are enriched in the proximity proteomes of $SOD1^{WT}$, relative to $SOD1^{G85R}$ and $SOD1^{G93A}$, respectively (Figure 1d). Gene ontology analysis for the enriched proteins showed several important pathways, including cytoplasmic translation, stress granule assembly, nucleosome assembly, chromatin silencing, mRNA

destabilization, and so forth (Figure S2). Along this line, several ribosomal proteins, including RPS10, RPS13, RPS14, RPS17, RPL23A, RPL26, and RPL27A, are enriched in the proximity proteome of $SOD1^{WT}$ only (Figure 1e).

XPO5 Displays Preferential Interactions with $SOD1^{G85R}$ and $SOD1^{G93A}$ over WT SOD1.

XPO5 is one of the most pronouncedly enriched proximity proteins of $SOD1^{G85R}$ and $SOD1^{G93A}$, and it is worth further investigation owing to its importance in small RNA transport and miRNA maturation.[20,21] We monitored the peak areas for one of the unique peptides of XPO5, that is, DPLLLAIIPK, identified from the proximity proteomes of $SOD1^{WT}$, $SOD1^{G85R}$, and $SOD1^{G93A}$. We found that the peak areas observed in the selected-ion chromatograms for the $[M + 2H]^{2+}$ ion of the peptide obtained for the proximity proteome samples of $SOD1^{G85R}$ and $SOD1^{G93A}$ were much larger than that of $SOD1^{WT}$, indicating stronger interactions of XPO5 with $SOD1^{G85R}$ and $SOD1^{G93A}$ than with $SOD1^{WT}$ (Figure S3a). In this vein, the sequence of the XPO5 peptide was supported by its MS/MS (Figure S3b).

To further validate the aforementioned findings, we constructed $SOD1^{WT}$-Flag, $SOD1^{G85R}$-Flag, and $SOD1^{G93A}$-Flag by fusing three tandem repeats of the Flag epitope tag to the C-terminus of the SOD1 variants, and performed co-immunoprecipitation using anti-Flag beads, followed by western blot analysis. Our results revealed much stronger interactions between XPO5 and $SOD1^{G85R}$-Flag/$SOD1^{G93A}$-Flag than $SOD1^{WT}$-Flag in both HEK293T and N2a neuroblastoma cells (Figure 2a–d). It is of note that there was a band detected at the XPO5 location in the control pull-down samples for HEK293T and N2a cells without plasmid transfection or with transfection of empty plasmid; nonetheless, the intensity of that band in these control samples is much weaker than what we observed for the mutant SOD1-Flag pull-down samples. Together, the above MS data and western blot results substantiate that XPO5 interacts preferentially with $SOD1^{G85R}$ and $SOD1^{G93A}$ than with $SOD1^{WT}$.

ALS-Associated SOD1 Mutants Modulate the Nucle-ocytoplasmic Transport of Pre-miRNA and miRNA Maturation.

miRNAs are essential single-stranded noncoding RNA molecules that function in RNA silencing and gene expression regulation.[22] One of the major established functions of XPO5 is to transport pre-miRNA from the nucleus to the cytosol, and the transported pre-miRNA is further processed into mature miRNA by Dicer.[20] Thus, we next asked whether the ectopic expression of ALS-associated mutants of SOD1 perturbs the nucleocytoplasmic transport of pre-miRNAs. Toward this end, we monitored several representative pre-miRNAs that are highly expressed in mice and humans,[23–25] including miR-let7b, miR-30a, and miR-143. Our results revealed that, when compared with cells with the ectopic expression of WT SOD1, the ectopic expression of the two mutants of SOD1 results in elevated distributions of pre-miR-let7b, pre-miR-30a, and pre-miR-143 in the nuclei, which are accompanied by their diminished presence in the cytosol (Figure 3a). In this regard, we assessed the purities of the nuclear and cytoplasmic fractions by western blot analysis. We found that, while the cytoplasmic fraction has ~9.5% contamination of nuclear proteins (as reflected by the lamin B signal), the nuclear fraction is free of contamination from the cytoplasmic fraction (Figure S4). Together, the above results suggest that the augmented interactions between mutant

SOD1 proteins and XPO5 suppress the latter's function in exporting pre-miRNA from the nucleus to the cytosol.

After export into the cytosol, pre-miRNAs are subjected to cleavage by Dicer to generate mature miRNAs.[26] Thus, we also examined how ectopic expressions of the WT and the two ALS-linked mutants of SOD1 modulate the levels of mature miRNAs. Our result from RT-qPCR analysis revealed that the relative levels of mature miR-30a, miR-let7b, miR-100, and miR-15a were significantly higher in cells with the ectopic expression of the SOD1 mutants than in cells expressing $SOD1^{WT}$ ($p < 0.05$) (Figure 3b).

DISCUSSION

ALS is a fatal neurodegenerative disease, and ALS patients manifest with the progressive loss of motor neuron functions, with about 2 to 3 years of survival time after the disease onset in most cases.[2] Neurons of ALS patients display abnormal protein aggregation, disturbance of proteostasis, and dysregulations in RNA metabolism.[1,8,27] In the latter respect, perturbations in miRNA biogenesis, alternative splicing, and RNA transport are now considered the major mechanisms underlying ALS pathogenesis. Many studies have substantiated that ALS-associated mutations in *TDP*43 and *FUS*, which are RNA-binding proteins, can alter RNA metabolism.[28,29] Additionally, ALS-linked mutants of SOD1 were shown to perturb indirectly the RNA metabolism by modulating the functions of TDP43.[30] *SOD*1 was the earliest identified gene mutated in ALS, and its mutations account for 20% of familial ALS and 5% of apparently sporadic ALS.[31,32] $SOD1^{G85R}$ and $SOD1^{G93A}$ are among the most well-studied ALS-associated mutations in SOD1, and both mutants are known to elicit protein aggregation and misfolding in cells.[8] To date, the protein interactomes for these two SOD1 mutants remain largely unexplored.

Here, we employed APEX labeling and label-free quantification using LC–MS/MS to examine the proximity proteomes for $SOD1^{WT}$, $SOD1^{G85R}$, and $SOD1^{G93A}$. We found that, when compared with $SOD1^{WT}$, 43 and 24 proteins were enriched in the proximity proteomes of $SOD1^{G85R}$ and $SOD1^{G93A}$, respectively (Figure 1d). GO analysis of the proteins preferentially enriched in the proximity proteomes of the two SOD1 mutants revealed their involvement in several important biological pathways (Figure S2).

Among the differentially enriched proximity proteins, XPO5 exhibits preferential binding with the two mutants of SOD1 (Figure S2). We validated the proteomic results by immunoprecipitation, followed by western blot analysis, where both $SOD1^{G85R}$ and $SOD1^{G93A}$ display much more robust interactions with XPO5 than $SOD1^{WT}$ in HEK293T cells (Figure 2a,b). Similar findings were made for N2a mouse neuroblastoma cells (Figure 2c,d). These results together revealed that XPO5 interacts preferentially with $SOD1^{G85R}$ and $SOD1^{G93A}$ than with $SOD1^{WT}$. In this regard, it is important to note the limitation of the immunoprecipitation method; that is, it does not support that the interactions between SOD1 mutants and XPO5 are direct. Future studies can be conducted using other techniques, for example, surface plasmon resonance and GST pull-down assay using purified recombinant proteins, to further examine whether XPO5 interacts directly with the SOD1 variants.

XPO5 is known to promote the nucleocytoplasmic transport of small endogenous RNAs, including pre-miRNAs.[20] Our real-time qPCR results revealed increased nuclear distributions and attenuated cytoplasmic distributions of pre-miRNAs, including pre-miR30a, pre-miR-let7a, and pre-miR-143 in cells expressing the two ALS-associated mutants of SOD1 than those expressing the WT protein (Figure 3a). This result supports that $SOD1^{G93A}$ and $SOD1^{G85R}$ may sequester XPO5, thereby rendering it unavailable for facilitating the export of pre-miRNAs from the nucleus to the cytosol (Figure 3c).

Transported pre-miRNAs in the cytosol are subjected to maturation by a multiprotein complex comprising of Dicer and its partners, Argonaute 2 (AGO2), TAR RNA-binding protein 2, and interferon-inducible double-stranded RNA-dependent protein kinase activator.[33] miRNAs play vital roles in many crucial biological processes, including, among others, gene silencing, RNA editing, RNA methylation, and RNA decay.[34] Recent studies showed that ALS-associated SOD1 mutations could perturb miRNA biogenesis and mRNA stability[28] and several miRNAs may serve as potential diagnostic biomarkers for ALS.[35] Thus, we also examined the consequences of the SOD1 mutations on miRNA maturation. Interestingly, we found that mature miR-30a, miR-let7b, miR-100, and miR-15a are present at higher levels in cells expressing the mutant SOD1 proteins than those expressing the WT counterpart (Figure 3b). At first glance, this finding appears to be incongruent with the fact that the expression of mutant SOD1 confers diminished levels of pre-miRNA in the cytosol for Dicer processing. However, aside from supporting the cytoplasmic export of pre-miRNAs, XPO5 exerts an inhibitory effect on Dicer when forming a complex with pre-miRNA and Ran-GTP.[21] Thus, the sequestration of XPO5 by SOD1 mutants forges the elevated activity of the Dicer complex, which leads to augmented miRNA maturation (Figure 3c). Previous studies revealed aberrant miRNA biogenesis in ALS-related pathologies,[33,36,37] and our results are in agreement with these studies. Importantly, our discovery of the interaction between XPO5 and the two mutants provides mechanistic insights into the roles of ALS-associated SOD1 mutants in miRNA biogenesis.

Apart from the identification of proteins exhibiting increased enrichment with the $SOD1^{G85R}$ and $SOD1^{G93A}$, our APEX labeling coupled with LC–MS/MS analysis also results in the identifications of 221 and 426 proteins being enriched in the proximity proteome of $SOD1^{WT}$ compared with $SOD1^{G85R}$ and $SOD1^{G93A}$, respectively (Figure 1e). Gene ontology analysis of the proteins exhibiting increased presence in the proximity proteome of $SOD1^{WT}$ showed the enrichment of several pathways, including stress granule formation, chromatin silencing, protein folding, chromatin silencing, and so forth (Figure S2). For instance, G3BP1 and TIA1 are important in stress granule formation,[38,39] and ARL2 and CDC37 are essential for protein folding[40,41] Future studies are needed to examine if the two SOD1 mutants elicit the loss of function of these pathways, which may also contribute to the development of ALS-associated pathologies.

In conclusion, we characterized comprehensively how two common ALS-linked mutations of SOD1 modulate its interaction proteomes and we uncovered, for the first time, XPO5 as an interaction partner of $SOD1^{G85R}$ and $SOD1^{G93A}$. The enhanced interaction between XPO5 and the SOD1 mutants led to attenuated nucleocytoplasmic transport of pre-miRNA and augmented levels of mature miRNAs. It will be interesting to explore, in the future,

how altered interactions with other cellular proteins conferred by the two SOD1 mutants contribute to the etiology of ALS.

Supplementary Material

Refer to Web version on PubMed Central for supplementary material.

ACKNOWLEDGMENTS

This work was supported by the National Institutes of Health (R35 ES031707).

REFERENCES

(1). Taylor JP; Brown RH; Cleveland DW Decoding ALS: from genes to mechanism. Nature 2016, 539, 197–206. [PubMed: 27830784]

(2). Kiernan MC; Vucic S; Talbot K; McDermott CJ; Hardiman O; Shefner JM; Al-Chalabi A; Huynh W; Cudkowicz M; Talman P; Van den Berg LH; Dharmadasa T; Wicks P; Reilly C; Turner MR Improving clinical trial outcomes in amyotrophic lateral sclerosis. Nat. Rev. Neurol 2021, 17, 104–118. [PubMed: 33340024]

(3). Ferraiuolo L; Kirby J; Grierson AJ; Sendtner M; Shaw PJ Molecular pathways of motor neuron injury in amyotrophic lateral sclerosis. Nat. Rev. Neurol 2011, 7, 616–630. [PubMed: 22051914]

(4). Renton AE; Chiò A; Traynor BJ State of play in amyotrophic lateral sclerosis genetics. Nat. Neurosci 2014, 17, 17–23. [PubMed: 24369373]

(5). Boillée S; Velde CV; Cleveland DW ALS: A Disease of Motor Neurons and Their Nonneuronal Neighbors. Neuron 2006, 52, 39–59. [PubMed: 17015226]

(6). Matsumoto G; Stojanovic A; Holmberg CI; Kim S; Morimoto RI Structural properties and neuronal toxicity of amyotrophic lateral sclerosis–associated Cu/Zn superoxide dismutase 1 aggregates. J. Cell Biol 2005, 171, 75–85. [PubMed: 16216923]

(7). Raoul C; Estévez AG; Nishimune H; Cleveland DW; deLapeyrière O; Henderson CE; Haase G; Pettmann B Motoneuron death triggered by a specific pathway downstream of Fas: Potentiation by ALS-linked SOD1 mutations. Neuron 2002, 35, 1067–1083. [PubMed: 12354397]

(8). Ross CA; Poirier MA Protein aggregation and neurodegenerative disease. Nat. Med 2004, 10, S10–S17. [PubMed: 15272267]

(9). Kim DI; Jensen SC; Noble KA; Kc B; Roux KH; Motamedchaboki K; Roux KJ An improved smaller biotin ligase for BioID proximity labeling. Mol. Biol. Cell 2016, 27, 1188–1196. [PubMed: 26912792]

(10). Lam SS; Martell JD; Kamer KJ; Deerinck TJ; Ellisman MH; Mootha VK; Ting AY Directed evolution of APEX2 for electron microscopy and proximity labeling. Nat. Methods 2015, 12, 51–54. [PubMed: 25419960]

(11). Branon TC; Bosch JA; Sanchez AD; Udeshi ND; Svinkina T; Carr SA; Feldman JL; Perrimon N; Ting AY Efficient proximity labeling in living cells and organisms with TurboID. Nat. Biotechnol 2018, 36, 880–887. [PubMed: 30125270]

(12). Hung V; Udeshi ND; Lam SS; Loh KH; Cox KJ; Pedram K; Carr SA; Ting AY Spatially resolved proteomic mapping in living cells with the engineered peroxidase APEX2. Nat. Protoc 2016, 11, 456–475. [PubMed: 26866790]

(13). Liu X; Yang Y-Y; Wang Y HSP90 and Aha1 modulate microRNA maturation through promoting the folding of Dicer1. Nucleic Acids Res 2022, 50, 6990–7001. [PubMed: 35736213]

(14). Perez-Riverol Y; Bai J; Bandla C; García-Seisdedos D; Hewapathirana S; Kamatchinathan S; Kundu DJ; Prakash A; Frericks-Zipper A; Eisenacher M; Walzer M; Wang S; Brazma A; Vizcaíno JA The PRIDE database resources in 2022: a hub for mass spectrometry-based proteomics evidences. Nucleic Acids Res 2022, 50, D543–D552. [PubMed: 34723319]

(15). Qin F; Shi X; Li H Separation of nuclear and cytoplasmic fractions for chimeric RNA characterization. Methods Mol. Biol 2020, 2079, 167–175. [PubMed: 31728970]

(16). Balcells I; Cirera S; Busk PK Specific and sensitive quantitative RT-PCR of miRNAs with DNA primers. BMC Biotechnol 2011, 11, 70. [PubMed: 21702990]

(17). Nel M; Mavundla T; Gultig K; Botha G; Mulder N; Benatar M; Wuu J; Cooley A; Myers J; Rampersaud E; Wu G; Heckmann JM Repeats expansions in ATXN2, NOP56, NIPA1 and ATXN1 are not associated with ALS in Africans. IBRO Neurosci. Rep 2021, 10, 130–135. [PubMed: 34179866]

(18). Todd TW; McEachin ZT; Chew J; Burch AR; Jansen-West K; Tong J; Yue M; Song Y; Castanedes-Casey M; Kurti A; Dunmore JH; Fryer JD; Zhang Y-J; San Millan B; Teijeira Bautista S; Arias M; Dickson D; Gendron TF; Sobrido M-J; Disney MD; Bassell GJ; Rossoll W; Petrucelli L Hexanucleotide Repeat Expansions in c9FTD/ALS and SCA36 Confer Selective Patterns of Neurodegeneration In Vivo. Cell Rep 2020, 31, 107616. [PubMed: 32375043]

(19). Atkin JD; Farg MA; Soo KY; Walker AK; Halloran M; Turner BJ; Nagley P; Horne MK Mutant SOD1 inhibits ER-Golgi transport in amyotrophic lateral sclerosis. J. Neurochem 2014, 129, 190–204. [PubMed: 24134191]

(20). Kim Y-K; Kim B; Kim VN Re-evaluation of the roles of DROSHA, Exportin 5, and DICER in microRNA biogenesis. Proc. Natl. Acad. Sci. U.S.A 2016, 113, No. E1881.

(21). Zeng Y; Cullen BR Structural requirements for pre-microRNA binding and nuclear export by Exportin 5. Nucleic Acids Res 2004, 32, 4776–4785. [PubMed: 15356295]

(22). Bartel DP MicroRNAs: Target recognition and regulatory functions. Cell 2009, 136, 215–233. [PubMed: 19167326]

(23). Zhao C; Sun G; Li S; Lang M-F; Yang S; Li W; Shi Y MicroRNA let-7b regulates neural stem cell proliferation and differentiation by targeting nuclear receptor TLX signaling. Proc. Natl. Acad. Sci. U.S.A 2010, 107, 1876–1881. [PubMed: 20133835]

(24). Maciejak A; Kostarska-Srokosz E; Gierlak W; Dluzniewski M; Kuch M; Marchel M; Opolski G; Kiliszek M; Matlak K; Dobrzycki S; Lukasik A; Segiet A; Sygitowicz G; Sitkiewicz D; Gora M; Burzynska B Circulating miR-30a-5p as a prognostic biomarker of left ventricular dysfunction after acute myocardial infarction. Sci. Rep 2018, 8, 9883. [PubMed: 29959359]

(25). Lagos-Quintana M; Rauhut R; Lendeckel W; Tuschl T Identification of Novel Genes Coding for Small Expressed RNAs. Science 2001, 294, 853–858. [PubMed: 11679670]

(26). Ha M; Kim VN Regulation of microRNA biogenesis. Nat. Rev. Mol. Cell Biol 2014, 15, 509–524. [PubMed: 25027649]

(27). Rozas P; Bargsted L; Martínez F; Hetz C; Medinas DB The ER proteostasis network in ALS: Determining the differential motoneuron vulnerability. Neurosci. Lett 2017, 636, 9–15. [PubMed: 27150076]

(28). Butti Z; Patten SA RNA dysregulation in amyotrophic lateral sclerosis. Front. Genet 2018, 9, 712. [PubMed: 30723494]

(29). Pham J; Keon M; Brennan S; Saksena N Connecting RNA-modifying similarities of TDP-43, FUS, and SOD1 with microRNA dysregulation amidst a renewed network perspective of amyotrophic lateral sclerosis proteinopathy. Int. J. Mol. Sci 2020, 21, 3464. [PubMed: 32422969]

(30). Jeon GS; Shim YM; Lee DY; Kim JS; Kang M; Ahn SH; Shin JY; Geum D; Hong YH; Sung JJ Pathological modification of TDP-43 in amyotrophic lateral sclerosis with SOD1 mutations. Mol. Neurobiol 2019, 56, 2007–2021. [PubMed: 29982983]

(31). Rosen DR; Siddique T; Patterson D; Figlewicz DA; Sapp P; Hentati A; Donaldson D; Goto J; O'Regan JP; Deng HX; Rahmani Z; Krizus A; McKenna-Yasek D; Cayabyab A; Gaston SM; Berger R; Tanzi RE; Halperin JJ; Herzfeldt B; Van den Bergh R; Hung WY; Bird T; Deng G; Mulder DW; Smyth C; Laing NG; Soriano E; Pericak–Vance MA; Haines J; Rouleau GA; Gusella JS; Horvitz HR; Brown RH Mutations in Cu/Zn superoxide dismutase gene are associated with familial amyotrophic lateral sclerosis. Nature 1993, 362, 59–62. [PubMed: 8446170]

(32). Kiernan MC; Vucic S; Cheah BC; Turner MR; Eisen A; Hardiman O; Burrell JR; Zoing MC Amyotrophic lateral sclerosis. Lancet 2011, 377, 942–955. [PubMed: 21296405]

(33). Emde A; Eitan C; Liou L-L; Libby RT; Rivkin N; Magen I; Reichenstein I; Oppenheim H; Eilam R; Silvestroni A; Alajajian B; Ben-Dov IZ; Aebischer J; Savidor A; Levin Y; Sons R; Hammond SM; Ravits JM; Möller T; Hornstein E Dysregulated miRNA biogenesis downstream of cellular

stress and ALS-causing mutations: a new mechanism for ALS. EMBO J 2015, 34, 2633–2651. [PubMed: 26330466]

(34). Ha M; Kim VN Regulation of microRNA biogenesis. Nat. Rev. Mol. Cell Biol 2014, 15, 509–524. [PubMed: 25027649]

(35). Parisi C; Arisi I; D'Ambrosi N; Storti AE; Brandi R; D'Onofrio M; Volonté C Dysregulated microRNAs in amyotrophic lateral sclerosis microglia modulate genes linked to neuroinflammation. Cell Death Dis 2013, 4, No. e959.

(36). Parisi C; Arisi I; D'Ambrosi N; Storti AE; Brandi R; D'Onofrio M; Volonté C Dysregulated microRNAs in amyotrophic lateral sclerosis microglia modulate genes linked to neuroinflammation. Cell Death Dis 2013, 4, No. e959.

(37). Zhang T; Wu YC; Mullane P; Ji YJ; Liu H; He L; Arora A; Hwang HY; Alessi AF; Niaki AG; Periz G; Guo L; Wang H; Elkayam E; Joshua-Tor L; Myong S; Kim JK; Shorter J; Ong SE; Leung AKL; Wang J FUS regulates activity of microRNA-mediated gene silencing. Mol. Cell 2018, 69, 787–801. [PubMed: 29499134]

(38). Yang PG; Mathieu C; Kolaitis RM; Zhang PP; Messing J; Yurtsever U; Yang ZM; Wu JJ; Li YX; Pan QF; Yu JY; Martin EW; Mittag T; Kim HJ; Taylor JP G3BP1 Is a tunable switch that triggers phase separation to assemble stress granules. Cell 2020, 181, 325–345. [PubMed: 32302571]

(39). Mackenzie IR; Nicholson AM; Sarkar M; Messing J; Purice MD; Pottier C; Annu K; Baker M; Perkerson RB; Kurti A; Matchett BJ; Mittag T; Temirov J; Hsiung GYR; Krieger C; Murray ME; Kato M; Fryer JD; Petrucelli L; Zinman L; Weintraub S; Mesulam M; Keith J; Zivkovic SA; Hirsch-Reinshagen V; Roos RP; Züchner S; Graff-Radford NR; Petersen RC; Caselli RJ; Wszolek ZK; Finger E; Lippa C; Lacomis D; Stewart H; Dickson DW; Kim HJ; Rogaeva E; Bigio E; Boylan KB; Taylor JP; Rademakers R TIA1 mutations in amyotrophic lateral sclerosis and frontotemporal dementia promote phase separation and alter stress granule dynamics. Neuron 2017, 95, 808–816. [PubMed: 28817800]

(40). Bhamidipati A; Lewis SA; Cowan NJ ADP ribosylation factor-like protein 2 (Arl2) regulates the interaction of tubulin-folding cofactor D with native tubulin. J. Cell Biol 2000, 149, 1087–1096. [PubMed: 10831612]

(41). Young JC; Agashe VR; Siegers K; Hartl FU Pathways of chaperone-mediated protein folding in the cytosol. Nat. Rev. Mol. Cell Biol 2004, 5, 781–791. [PubMed: 15459659]

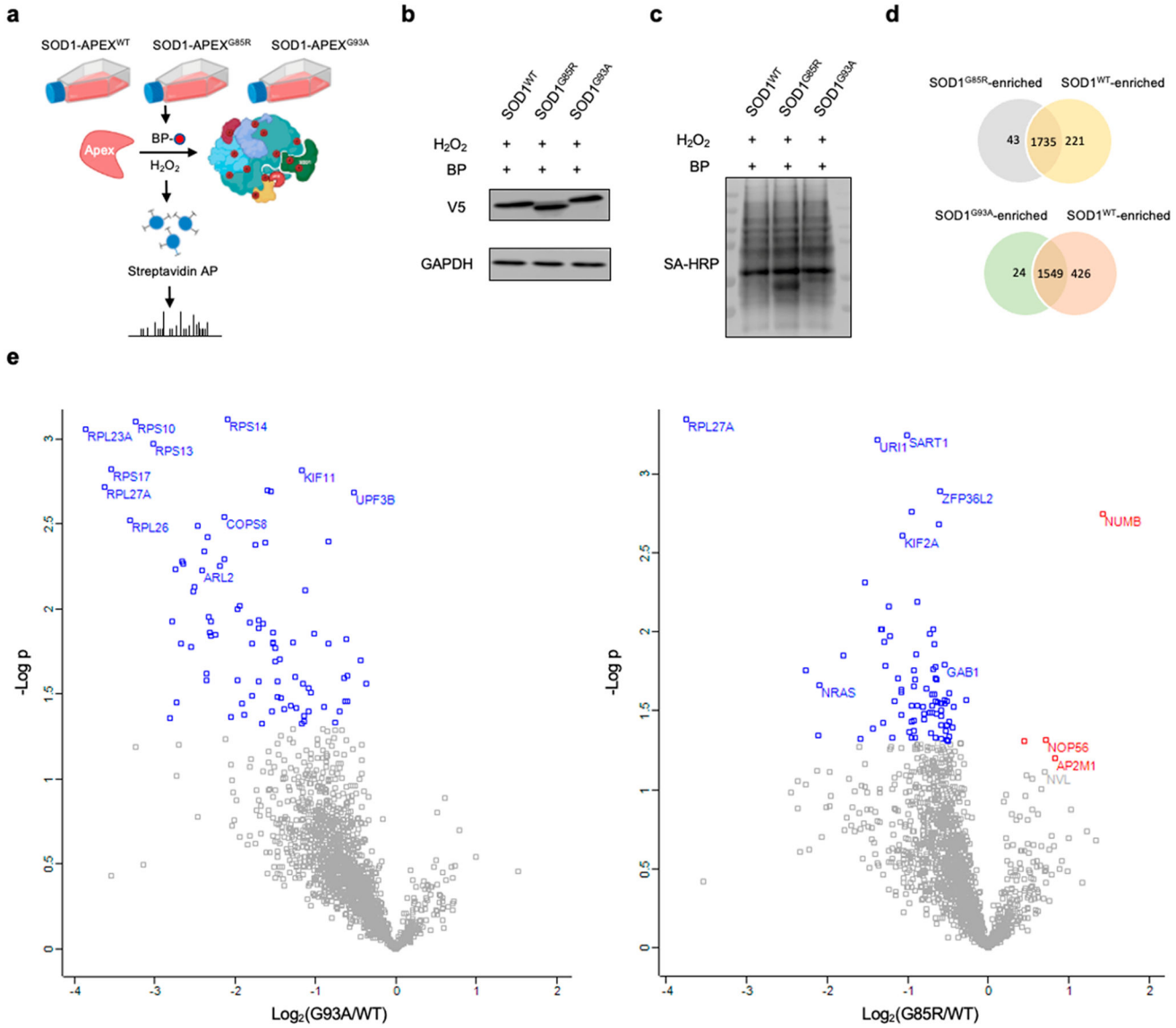

Figure 1.

Combination of APEX2 labeling with LC–MS/MS revealed XPO5 as a candidate interaction partner of SOD1^{G85R} and SOD1^{G93A}. (a) Schematic diagram showing the workflow for APEX labeling. “BP” and “AP” represent biotin phenol and affinity pull-down, respectively. (b) Western blot showing a similar level of expression for different SOD1-APEX2 variants in HEK293T cells. (c) Western blot indicated similar APEX labeling efficiencies for SOD1^{WT}, SOD1^{G85R}, and SOD1^{G93A}. Cells were transfected with plasmids encoding APEX2-conjugated SOD1^{WT}, SOD1^{G85R}, and SOD1^{G93A} for 24 h, followed by treatments with biotin phenol for 30 min and then with H_2O_2 for 1 min. “SA-HRP” represents streptavidin-horseradish peroxidase. (d) Venn diagrams comparing the proximity proteomes of SOD1^{G85R} vs SOD1^{WT} and SOD1^{G93A} vs SOD1^{WT}. In total, 1999 proteins were identified. (e) Volcano plots displaying fold changes for the proteins being pulled down with streptavidin beads. The *p* values were calculated by using paired, two-tailed Student’s

t-test. The red and blue labels designate those with statistically significant fold changes ($p < 0.05$).

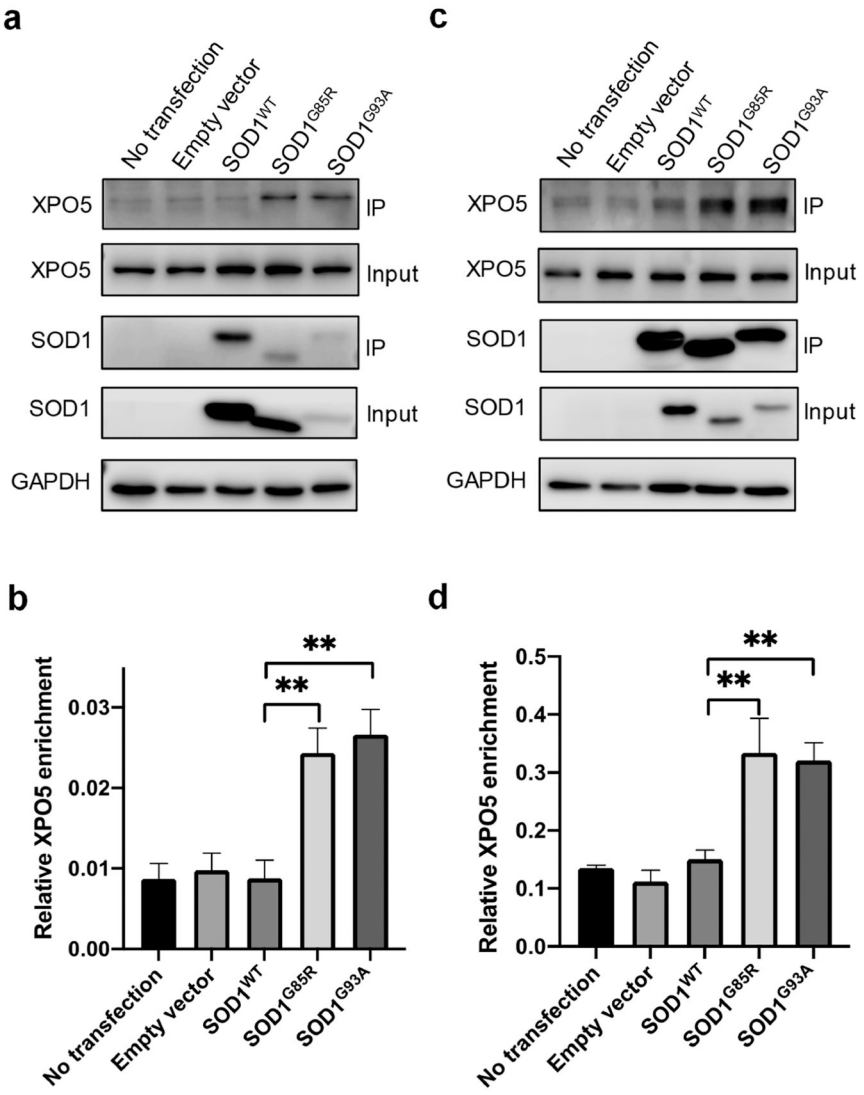

Figure 2.

Immunoprecipitation followed by western blot analysis revealed stronger interactions between XPO5 and $SOD1^{G85R}$/$SOD1^{G93A}$ than $SOD1^{WT}$ in HEK293T and N2a cells. (a,c) HEK293T and N2a cells were transfected with the empty vector (pRK7), $SOD1^{WT}$-Flag, $SOD1^{G85R}$-Flag, and $SOD1^{G93A}$-Flag for 24 h, and the resulting lysates were incubated with anti-Flag beads for 2 h. Western blot was used to monitor the interaction between XPO5 and the three Flag-tagged proteins. (b,d) The relative enrichment of XPO5 (a,c) was quantified using Image Studio based on the band intensities of XPO5 in the IP samples and normalized to those of XPO5 in the corresponding input samples ($n = 3$). The p values were calculated using one-way ANOVA: *, $0.01 \leq p < 0.05$; **, $0.001 \leq p < 0.01$; ***, $p < 0.001$.

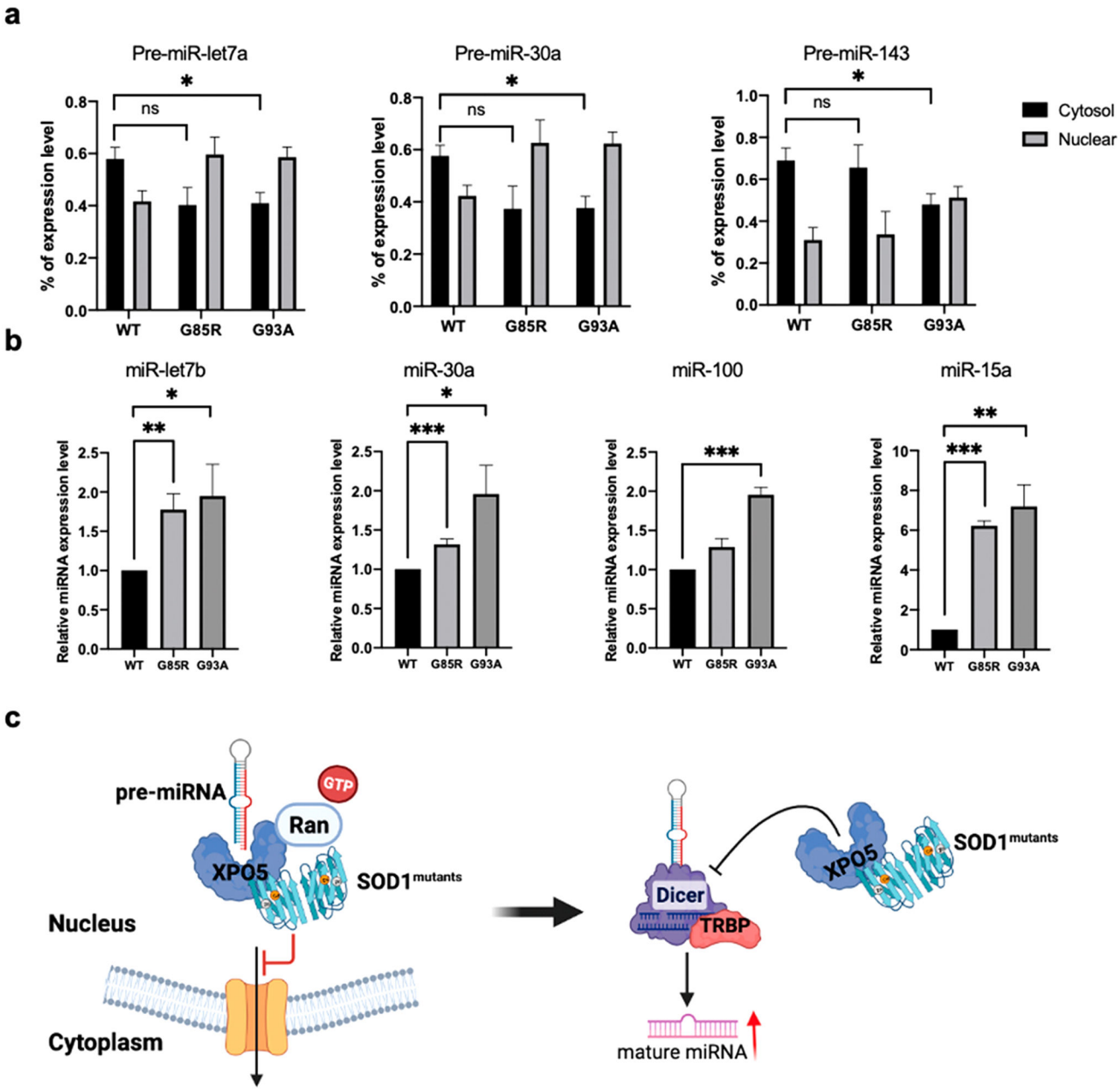

Figure 3.

Ectopic expression of the G85R and G93A mutants of SOD1 perturbs the nucleocytoplasmic transport of pre-miRNAs and the maturation of miRNAs. (a) RT-qPCR results showing increases in the nuclear levels and decreases in the cytosol levels of pre-miR-let7a, pre-miR-30a, and pre-miR-143 in cells expressing $SOD1^{G93A}$ and $SOD1^{G95R}$ compared to those expressing the WT protein. (b) RT-qPCR results depicting substantially increased levels of mature miR-30a, miR-let7b, miR-100, and miR-15a in cells with the ectopic expression of $SOD1^{G85R}$ and $SOD1^{G93A}$ than those with $SOD1^{WT}$. (c) Schematic diagram illustrating the inhibitory effect of ALS-associated SOD1 mutants on XPO5-mediated nucleocytoplasmic transport of pre-miRNAs and on diminished inhibitory effects of XPO5 toward the Dicer-

mediated cleavage of pre-miRNAs to mature miRNAs. All data were normalized to the mRNA level of *GAPDH*. The *p* values were calculated using unpaired, two-tailed Student's *t*-test: ns, not significant ($p > 0.05$); *, $0.01 \leq p < 0.05$; **, $0.001 \leq p < 0.01$; ***, $p < 0.001$.